ACS OMEGA

http://pubs.acs.org/journal/acsodf

Article

Ni-Decorated PtS_2 Monolayer as a Strain-Modulated and Outstanding Sensor upon Dissolved Gases in Transformer Oil: A First-Principles Study

Zhuoli Xu*

Cite This: *ACS Omega* 2023, 8, 6090−6098

Read Online

ACCESS | Metrics & More | Article Recommendations

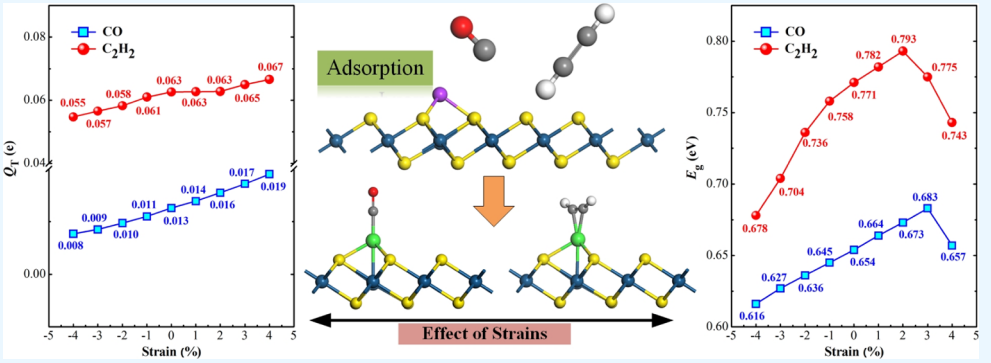

ABSTRACT: The first-principles theory is conducted in this paper to investigate the adsorption and electronic properties of a Ni-decorated PtS_2 (Ni-PtS_2) monolayer upon two dissolved gas species (CO and C_2H_2) in the transformer oil, thus illustrating its sensing performance and related potential to evaluate the working condition of the oil-immersed transformers. We then highlight the effect of the biaxial strain on the configuration, charge transfer, and bandgap of the adsorbed systems to expound its potential as a strain-modulated gas sensor. Results indicate that the Ni-PtS_2 monolayer undergoes chemisorption upon two species, with an E_{ad} value of −1.78 eV for the CO system and −1.53 eV for the C_2H_2 system. The reduced bandgap by 0.164 eV (20.05%) in the CO system and 0.047 eV (5.74%) in the C_2H_2 system imply the large feasibility of the Ni-PtS_2 monolayer to be a resistance-type sensor for CO and C_2H_2 detection, which is also verified by the $I-V$ analysis of these systems. Besides, the applied biaxial strain can exert geometric activations on the Ni-PtS_2 monolayer, and specifically, the compressive force can further reduce the bandgap in two systems, thus promoting its sensing response upon two gases. Our work is meaningful to broaden the exploration of noble transition metal dichalcogenides for gas sensing.

1. INTRODUCTION

Electrical transformers play a significant role in the power system to transform and transmit the electricity in the transmission lines, among which oil-immersed transformers account for over 90% at present.[1] In a long-time running, there may inevitably occur certain insulation defect inner transformers,[2,3] namely, partial overheat and partial discharge, and the energy caused by these defects would decompose the oil−paper system of the transformers, impairing its insulation behavior accordingly.[4] As reported, the decomposed compounds mainly include H_2, C_2H_2, and CO, which will then dissolve into the transformer oil after their formation.[5,6] Therefore, dissolved gas analysis (DGA) is put forward to reflect the decomposition severity of the oil−paper system and to evaluate the operating condition of the transformers.[7,8] From this regard, the scholars devote every effect to explore a certain effective sensing method to realize DGA, giving rise to the safety operation and daily maintenance of the oil-immersed transformers.[9,10]

Nanosensing method for gas detection has proved with the advantages of quick response, good sensitivity, and low cost,[11−14] and 2D nanomaterials with the merits of large specific surface and high carrier mobility usually show favorable adsorption performance in the gas interactions, thus leading to the desirable electrical response for gas detection.[15−18] Nowadays, transition metal dichalcogenides (i.e., TMDs) with strong potential to be the 2D nanoelectronic candidates are paid more

Received: January 2, 2023
Accepted: January 24, 2023
Published: February 1, 2023

https://doi.org/10.1021/acsomega.3c00022
ACS Omega 2023, 8, 6090−6098

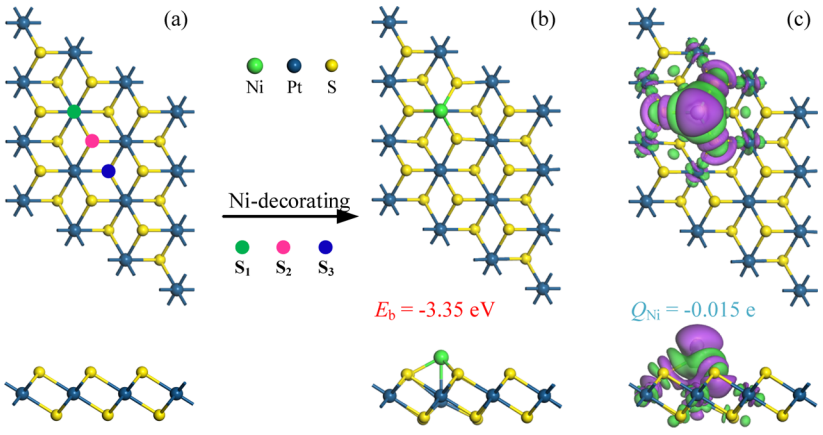

Figure 1. Ni decorating on the PtS_2 monolayer. (a) Pure PtS_2 and (b,c) geometry and CDD of Ni-PtS_2. In CDD, the green area is the electron accumulation, and the rosy areas is electron depletion, respectively. The isosurface is set as 0.005 eV/Å^3.

and more attention in the field of gas sensing.[19−21] For example, MoS_2 and $MoSe_2$ have been proposed for DGA with superior sensing performance upon CO and C_2H_2 after the surface doping of the transition metal (TM).[22,23]

Increasingly, PtS_2 and $PtSe_2$ as new members of the TMDs are synthesized and predicted with diverse electronic property compared with those of MoS_2 and $MoSe_2$.[24−27] Specifically, the PtS_2 monolayer has indirect semiconducting property with much stronger elastic constant than that of the MoS_2 monolayer[28] and larger electron mobility than the black phosphorus.[29] This provides the PtS_2 monolayer with strong potential for application in nanoelectronics with tunable performance through strain engineering. Besides, TM doping offers a workable approach to promote the charge transfer in the gas interactions, thereby enhancing the sensing response for gas detection.[30−35] From this aspect, the TM-doped PtS_2 monolayer would be full of potential for gas sensing application, and its exploration for DGA would be interesting and meaningful.

In this paper, the Ni-decorated PtS_2 (i.e., Ni-PtS_2) monolayer is proposed to be a novel strain-modulated sensor for detections of CO and C_2H_2 in the oil-immersed transformer using the first-principles theory.[36] A Ni atom is selected as the dopant due to its strong catalytic behavior that frequently brings high sensitivity to the 2D nanosensing systems for gas detection.[37−40] Also, Ni is the representative TM dopant to analyze the TM-decorating performance on the physicochemical properties of the PtS_2 monolayer. Our calculations can pave the way to explore PtS_2-based strain-tuned sensors for gas detections in many others fields.

2. COMPUTATIONAL METHODS

In this paper, all the spin-polarized calculations were performed in the DMol^3 package,[41] and the generalized gradient approximation along with the Perdew−Burke−Ernzerhof (PBE) function was determined to describe the electron-exchange correlations.[42] The DFT-D2 method raised by Tkatchenko and Scheffler (TS) was adopted to treat the van der Waals force as well as the long-range interactions,[43] and the double-numerical plus polarization was determined as the basic atomic orbital set throughout the whole simulations.[44] The 10 × 10 × 1 *k*-point meshes of the Monkhorst−Pack was sampled for the geometric optimization and electronic calculations.[45] The energy tolerance accuracy (energy convergence) and smearing were defined as 10^{-5} and 0.005 Ha, respectively,[46] with the global orbital cut-off radius set as 5.0 Å to enable the good accuracy of the total energy.[47]

A 3 × 3 × 1 pristine PtS_2 supercell was used as the nanosupport to implement the following simulations, with a vacuum area of 20 Å to avoid the probable interactions.[31,48] After full geometry optimization, it is found that the lattice constant of the intrinsic PtS_2 system was procured to be 3.58 Å, consistent with that of 3.59 Å in ref 49 . Moreover, the charge of the Ni atom (Q_{Ni}) in the Ni-decorating process as well as the charge transfer (Q_T) in the gas-adsorbed configurations were considered by the Hirshfeld analysis. Based on such method, the positive *Q* implied the charge-donating behavior of the analytes.

3. RESULTS AND DISCUSSION

3.1. Ni-Decorating Property on the PtS_2 Monolayer.

For Ni decorating on the pristine PtS_2 monolayer, there are three probable sites for consideration, as displayed in Figure 1a, wherein one Ni atom is adsorbed on the PtS_2 surface to form the Ni-PtS_2 structure. In the meanwhile, the binding energy (E_b) is applied to reflect the binding force for Ni decorating on the PtS_2 surface, calculated as

$$E_b = E_{Ni-PtS_2} - E_{Ni} - E_{PtS_2} \quad (1)$$

wherein $E_{Ni\text{-}PtS_2}$, E_{Ni}, and E_{PtS_2} are, respectively, the total energies of the Ni-PtS_2 monolayer, one Ni atom, and the intrinsic PtS_2 system.

With the fully optimized configurations, we find that the most stable Ni-decorating site on the pristine PtS_2 surface is through the S1 position, as depicted in Figure 1b wherein the Ni dopant is trapped by three S atoms and right above the middle-layered Pt atom. One can see that the Ni adatom is captured by three S atoms and one middle-layered Pt atom of the PtS_2 surface, forming three Ni−S bonds with an equivalent bond length of 2.19 Å and one Ni-Pt bond with a bond length of 2.59 Å. The E_b value for the S1 site is procured to be −3.35 eV, which is more negative than that of −1.85 eV in the S2 site and that of −3.05 eV in the S3 site. Such findings suggest that the Ni adatom could be stably anchored on the PtS_2 surface with strong binding force with the S and Pt atoms. Accordingly, some Pt−S bonds, especially those around the Ni dopant, are somewhat deformed after Ni-doping elongating from 2.41 to 2.42−2.44 Å. This indicates the geometric activation of the PtS_2 monolayer caused by the Ni doping.[50] From the vibrational analysis, it is found that the frequencies of the Ni-PtS_2 monolayer are ranging at 99.12−

https://doi.org/10.1021/acsomega.3c00022
ACS Omega 2023, 8, 6090−6098

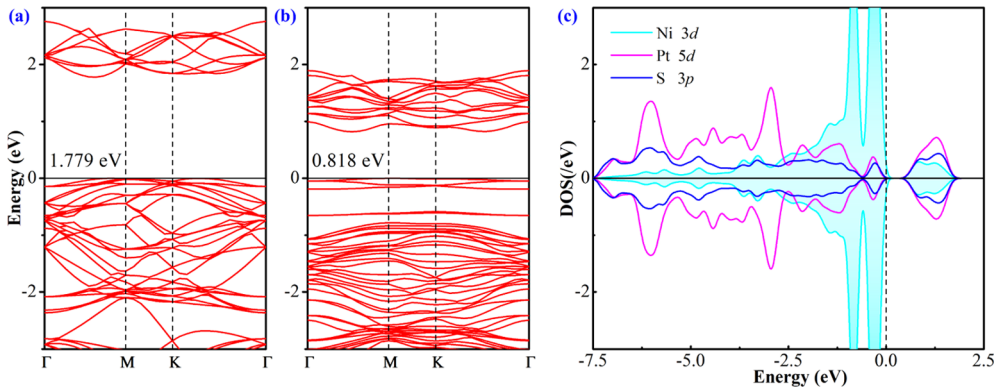

Figure 2. BS and DOS of the Ni-PtS_2 monolayer. (a,b) BS of the pure and Ni-doped $PtSe_2$ system and (c) orbital DOS of bonded atoms. In the BS, the black values are the bandgaps, while in DOS, the dashed line is the Fermi level.

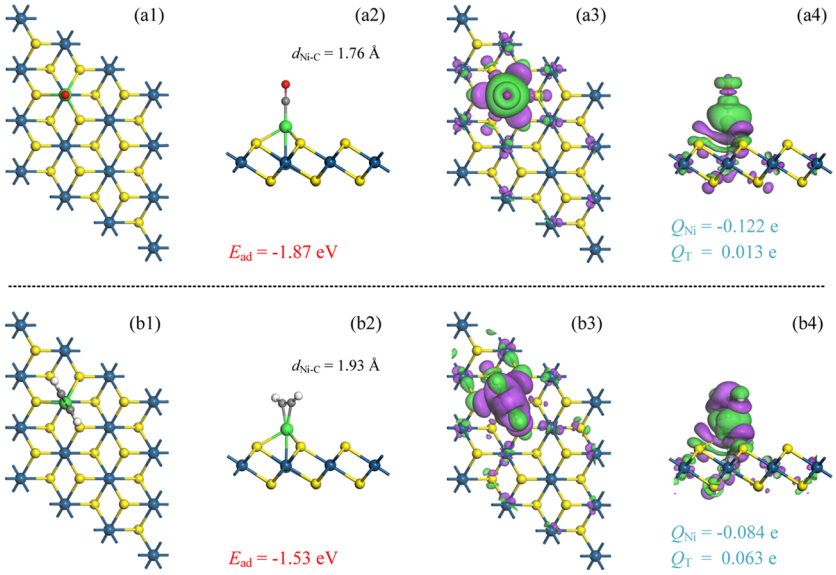

Figure 3. MSC and related CDD of (a) CO system and (b) C_2H_2 system. The isosurface set in the CDD is the same as in Figure 1.

1011.64 cm^{-1}, without the imaginary frequency indicating the good chemical stability of such configuration.

Using the Hirshfeld method, it is found that the Ni adatom is charged by −0.015 e, indicating the electron-withdrawing behavior of the Ni dopant when interacting with the PtS_2 surface. Moreover, from Figure 1c, wherein the charge density difference (i.e., CDD) of Ni-PtS_2 system is plotted, it is found that there are strong electron accumulations on the Ni−Pt and Ni−S bonds, which reveal the electron localization on these newly formed bonds, indicating the firm binding forces between related atoms.

Figure 2 displays the band structure (BS) in parallel with density of state (DOS) of the Ni-PtS_2 monolayer to illustrate the Ni-decorating performance on the electronic properties of the pristine PtS_2 system. Also, one can see from Figure 2a that the bandgap of the pristine PtS_2 monolayer is obtained to be 1.779 eV using the PBE function, and those using the PBEsol and HCHT function are obtained as 1.810 and 1.858 eV, respectively. From these results, one can find that different functions can give rise to different bandgaps for the same system, and in this work, the bandgap using the PBE function is in good agreement with that of 1.77 eV in the previous report;[51] therefore, we will use such function in the following simulations. As exhibited in Figure 2b, the bandgap of the Ni-PtS_2 system is obtained as 0.818 eV, much smaller than that in the pristine counterpart. Besides, it could be observed that the states in the BS are down-shifted, and there are several impurity states emerged within the bandgap of the PtS_2 monolayer. In other words, Ni-doping induces some impurity states and causes slight n-doping for the PtS_2 monolayer. On the other hand, its indirect semiconducting property is not impacted, although its states become much denser, manifesting the improved carrier mobility of the Ni-PtS_2 monolayer. Figure 2c shows the orbital DOS of the Ni, Pt, and S atoms, from which one can see that the Ni 3d orbital has strong hybridizations with Pt 5d and S 3p orbitals on −6.0 to 0 and 0.5−1.6 eV. Such DOS overlaps indicate the powerful orbital interactions between the Ni dopant and the Pt (S) atom, thus forming the Ni−Pt and Ni−S bonds on which the electron hybridizations are happened. In addition, the top valence band is dominantly located at the Ni atom, whereas the bottom conduction bond is dominantly located at the Pt atom, followed by the S atom. These results reveal the chemical bonding nature for the Ni−Pt and Ni−S and the their strong orbital hybridization as well.[52]

3.2. Adsorption Performance of the Ni-PtS_2 Monolayer. The binding strength of the Ni-PtS_2 monolayer upon CO and C_2H_2 molecules is reflected by the defined adsorption energy (E_{ad}), calculated as

https://doi.org/10.1021/acsomega.3c00022
ACS Omega 2023, 8, 6090−6098

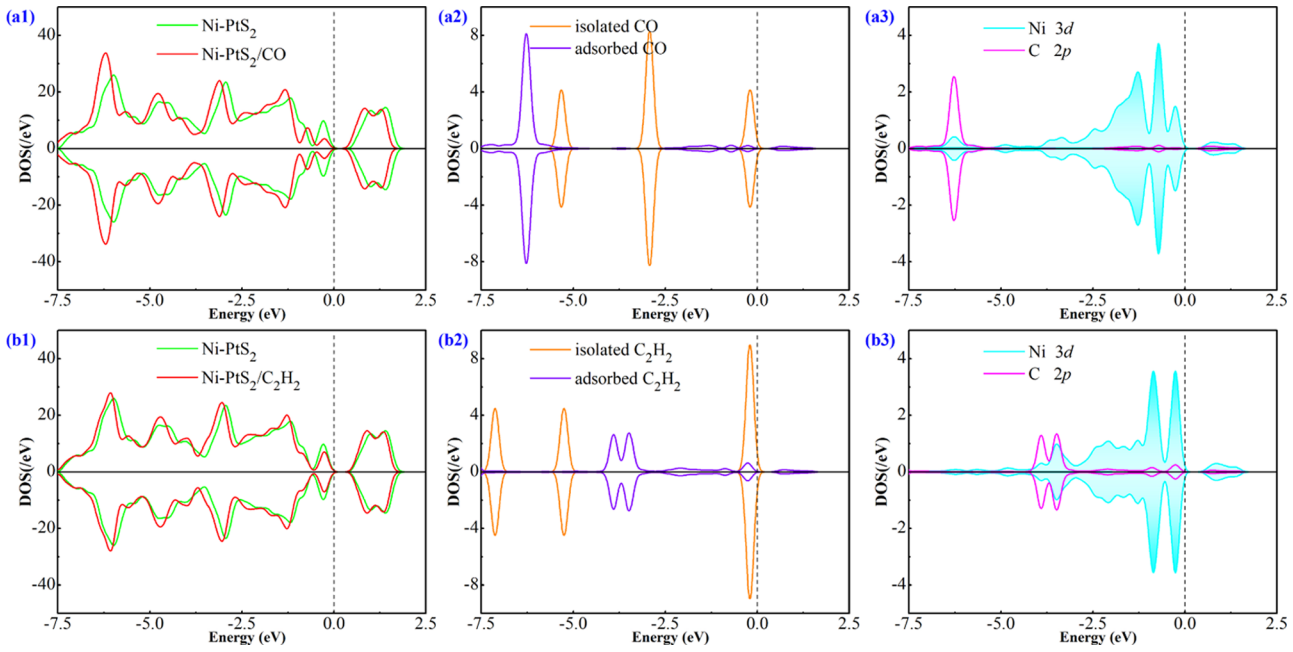

Figure 4. DOS of the (a1−a3) CO system and the (b1−b3) C_2H_2 system. The dashed line is the Fermi level.

$$E_{ad} = E_{Ni-PtS_2/gas} - E_{Ni-PtS_2} - E_{gas} \quad (2)$$

where $E_{Ni\text{-}PtS_2/gas}$, $E_{Ni\text{-}PtS_2}$, and E_{gas}, respectively, signify the total energies of the Ni-PtS_2/gas system, isolated Ni-PtS_2 monolayer, and the gas species. The gas molecules are put appropriate 2.5 Å to the Ni center in various structures to obtain the most stable configuration (i.e., MSC that has the most negative E_{ad}) of the gas-adsorbed systems. In the meanwhile, the parameters of bond length and charge transfer would also be analyzed to help comprehend the adsorption performance of the Ni-PtS_2 monolayer. We should note that for dissolved gas detection, the targeted gases are extracted to the vacuum environment and perform the gas sensing process. Therefore, in this section, we directly analyze the gas adsorption processes without considering the impact of humidity or oxygen.

The MSC and related CDD for CO and C_2H_2 adsorptions onto the Ni-PtS_2 surface are exhibited in Figure 3. We should initially mention that the frequencies of CO and C_2H_2 systems are obtained as 61.12−2360.60 and 99.77−3470.30 cm^{-1}, respectively, which suggest their good chemical stability. Upon the CO adsorption system, it is found that the CO molecule tends to be captured directly on top of the Ni dopant standing vertical to the PtS_2 layer, forming a Ni−C bond of 1.76 Å, and the C≡O bond is prolonged to 1.16 Å, from 1.14 Å in its gas phase, the average length of the Ni−Pt bond prolongs to 2.31 Å, and the Ni−S bonds shorten to 2.58 Å. These bond deformations manifest the structural activation upon the adsorbed molecule and the Ni-PtS_2 surface caused by adsorption. The E_{ad} in the CO system is obtained as −1.87 eV, giving rise to the chemical adsorption nature here.[53] Besides, using the Hirshfeld analysis, the Q_T is procured as 0.013 e, which means that the CO molecule performs as an electron contributor releasing 0.013 e to the Ni-PtS_2 monolayer. Combined with the negatively charge Ni dopant of 0.122 e, one can infer that 0.094 e is transferred from the PtS_2 surface to the Ni dopant in CO adsorption. That is, the Ni adatom is an electron center-withdrawing electron from both the CO molecule and the PtS_2 surface. This would be beneficial for the electrostatic attraction between the Ni dopant and the CO molecule and thus promote the binding strength here. From the CDD, one can see that there are strong electron accumulations on the Ni−C bond, suggesting its strong biding force caused by the orbital hybridization, and there is electron depletion on the C≡O bond and the Ni−Pt bond, suggesting their weakness after gas adsorption.

In the MSC of the C_2H_2 system, it is found that C_2H_2 is captured by the Ni adatom via a molecule-parallel configuration, wherein both C atoms are bonded with the Ni dopant with an equivalent bond length of 1.93 Å. In the meanwhile, the C−H bond in the C_2H_2 molecule is somewhat distorted upward, bending such molecule from its linear configuration. Besides, the C═C bond elongates to 1.26 from 1.21 Å in the isolated C_2H_2 gas phase, and Ni−Pt and Ni−S bonds are, respectively, prolonged to 2.37 and 2.62 Å. Such structural activations imply the admirable binding forces between the Ni dopant and the C_2H_2 molecule, thus leading to the large E_{ad} of −1.53 eV. From this aspect, chemisorption can be identified as well for the C_2H_2 system. On the basis of the Hirshfeld analysis, C_2H_2 as a whole is charged by 0.063 e, which indicates its electron-donating behavior in gas interactions.[54] At the same time, the Ni adatom is negatively charged by 0.084 e. Thus, one can deduce that the PtS_2 monolayer transfers 0.006 e to the Ni dopant in C_2H_2 adsorption. That is, the Ni dopant has strong electron-accepting property in gas interactions, consistent with that in the H_2 system accepting electron from both the gas molecule and the PtS_2 surface. From the CDD distribution, the electron hybridizations could be seen on the Ni−C bonds, while electron depletions could be seen on the C═C and Ni−Pt bonds. These results are in accordance with the analysis of geometric activations for the C_2H_2 molecule and the Ni-PtS_2 monolayer caused by gas adsorption.

3.4. Electronic Property of Gas Adsorption Systems.

The above analyses indicate that chemisorption is identified for both CO and C_2H_2 systems, in which two gases behave as electron donators causing the electron distribution in the whole systems. From this regard, the electronic properties of the Ni-

https://doi.org/10.1021/acsomega.3c00022
ACS Omega 2023, 8, 6090−6098

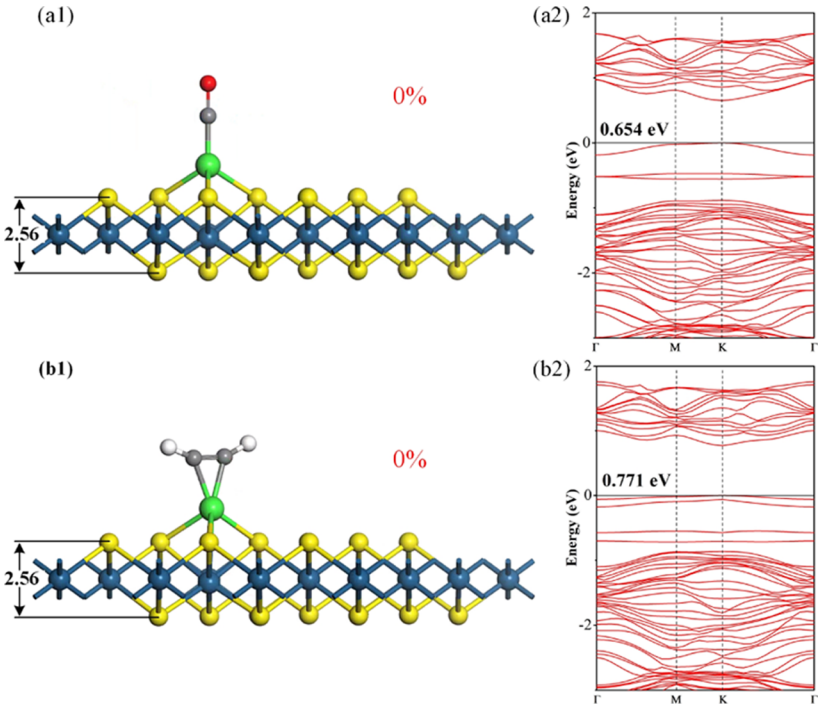

Figure 5. MSC and BS of the CO system (a1,a2) and C_2H_2 system (b1,b2) under 0% applied biaxial strains. The black values in MSC are the S−S layer distance, unit in Å, while the black values in BS are the bandgap of related systems.

PtS_2 system will be impacted, which can provide the sensing evidence of change in the electrical conductivity for gas detection. In this section, the DOS of the gas-adsorbed systems are portrayed in Figure 4 to help comprehend the electronic properties of the Ni-PtS_2 monolayer upon gas adsorptions.

Regarding the total DOS, the states of the gas adsorption systems are significantly diverse from those of the isolated Ni-PtS_2 system, which attributes to the state contributions of the adsorbed gases after electronic activation. While the Fermi level is originally defined at the top valence band within DMol^3 calculations, the bottom conduction band is somewhat left-shifted in the CO system and is slightly left-shifted in the C_2H_2 system. These results indicate the narrowed bandgap of the Ni-PtS_2 monolayer after adsorptions of two gas species. The electronic activation of the gas molecule after adsorption could be found in the molecular DOS. One can see that the states of the isolated CO and C_2H_2 molecule at the −0.5 eV are split into several small states surrounding the Fermi level in their adsorbed systems. It is these redistributed states of the adsorbed gases that contribute to the deformation of the total DOS. Moreover, the state hybridizations between the Ni 3d orbital and the C 2p orbital, at −6.6, −0.9, and 1.0 eV in the CO system and at −4.0, −3.5, −0.3, and 0.8 eV in the C_2H_2 system, as shown in the orbital DOS illustrate the orbital interaction in the formed Ni−C bonds which accounts for its strong binding force.[55]

3.5. Sensor Exploration and Effect of Strain. The change of electronic properties of the Ni-PtS_2 monolayer after gas adsorptions can further impact the change of some detectable electrical signals from a macroprospective,[56] for example, the electrical conductivity that can be reflected by the bandgap of the sensing material by[57]

$$\sigma = \lambda \cdot e^{(-B_g/2kT)} \quad (3)$$

wherein B_g is the bandgap, λ is a constant, T is the temperature, and k is the Boltzmann constant. From formula 3, it could be inferred that the larger bandgap accounts for the smaller electrical conductivity, thus leading to the larger electrical resistance for the gas sensor. Since the applied biaxial strain can also impact the bandgap of the PtS_2 monolayer,[28] we herein study the bandgap of the Ni-PtS_2 monolayer in the CO and C_2H_2 systems to illustrate its unique sensing performance for gas detection. The strain is defined as

$$\varepsilon = (a_0 - a)/a \quad (4)$$

in which a_0 and a are constant lattices of the Ni-PtS_2 monolayer with and without biaxial strains.

Figure 5 portrays the MSC without applied biaxial strain (same as Figure 3 but from a different view) and related BS of the CO and C_2H_2 systems. From the MSC with 0% biaxial strain, it is found that the S−S layer distance is measured to be 2.56 Å, which can be regarded as the base value for comparison with those in the strain-modulated systems. Besides, one can see from the BS that the bandgap of the Ni-PtS_2 monolayer is declined to diverse levels after CO and C_2H_2 adsorptions, specifically declining to 0.654 and 0.771 eV, from that of 0.818 eV for the pure counterpart. That is, the bandgap of Ni-PtS_2 system is reduced by 0.164 eV (20.05%) in the CO system and by 0.047 eV (5.74%) in the C_2H_2 system, respectively. Therefore, the electric conductivity of the Ni-PtS_2 monolayer can increase to different levels after CO or C_2H_2 adsorption, with larger increase in the CO system. This gives the basic sensing mechanism to explore the Ni-PtS_2 monolayer to be the resistance-type sensor for sensitive detections of two gas species,[58] especially upon CO. However, the selective detection between CO and C_2H_2 might not be realized effectively by such sensor given the same increasing trend in the conductivity of the Ni-PtS_2 monolayer upon two gaseous species.

Moreover, the recovery time is also important to identify the reusability of the Ni-PtS_2 monolayer as a gas sensor, which can be calculated using the van't-Hoff−Arrhenius theory[59] in eq 5

https://doi.org/10.1021/acsomega.3c00022
ACS Omega 2023, 8, 6090−6098

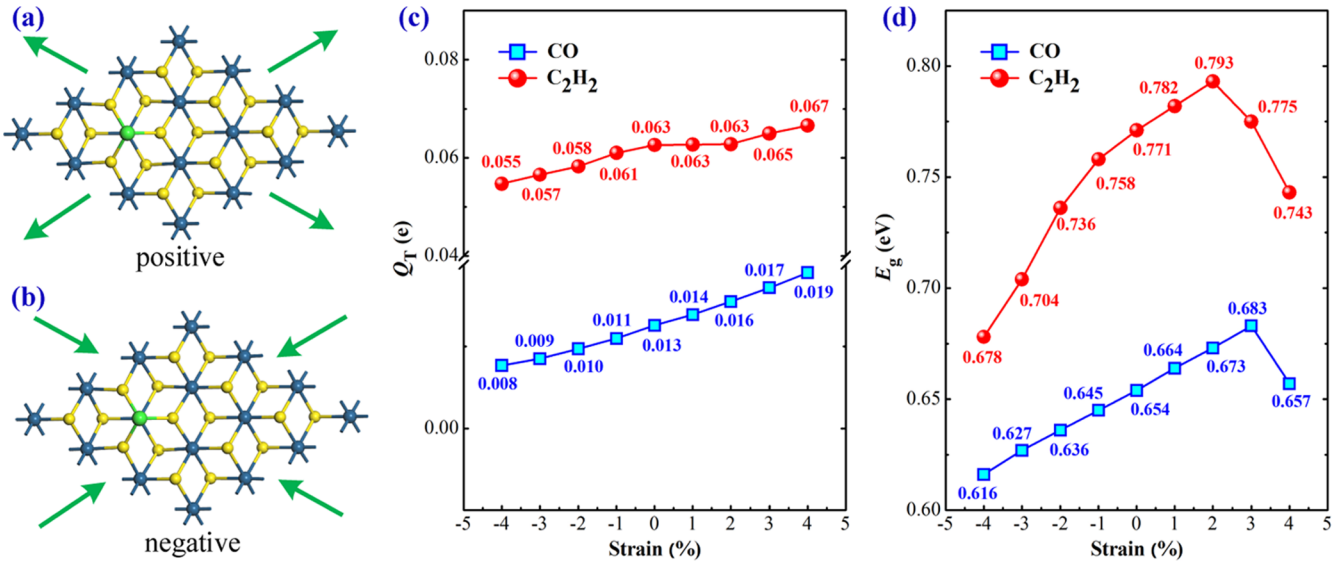

Figure 6. Effect of applied biaxial strain on Q_T and B_g upon gas adsorption. (a,b) Direction of the applied biaxial strain (c,d) variation of Q_T and B_g in gas-adsorbed systems.

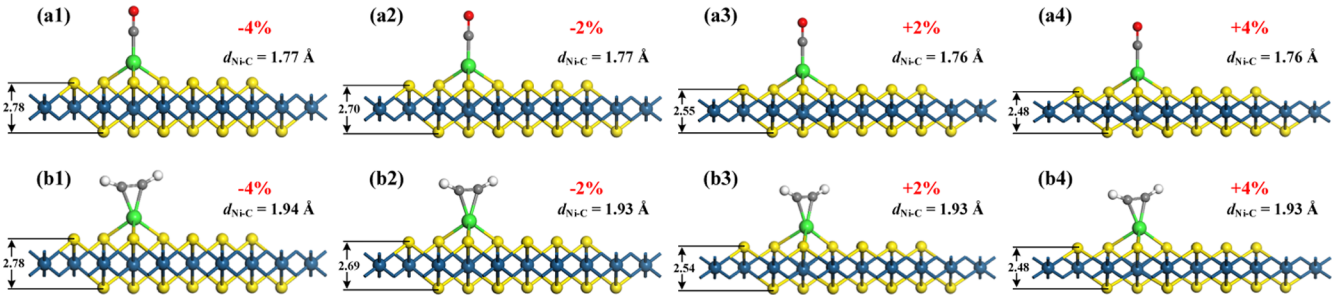

Figure 7. MSC of (a1−a4) CO system and (b1−b4) C_2H_2 system under the biaxial strains varying from −4 to +4%. The red values are the applied biaxial strains, while the black values are the S−S layer distance, unit in Å.

$$\tau = A^{-1} e^{(-E_{ad}/K_B T)} \quad (5)$$

in which K_B is the Boltzmann constant, as 8.318×10^{-3} kJ/(mol·K), A is the attempt frequency, as 10^{12} s^{-1}[60] in this work, and T is the temperature. Using eq 5, the recovery time (τ) in CO and C_2H_2 systems at room temperature is calculated as 4.10×10^{19} and 7.33×10^{13} s, respectively, and at 498 K is calculated as 8.26×10^{16} and 3003 s, respectively. These findings reveal that heating is a workable approach to make the Ni-PtS_2 gas sensor reusable for gas sensing. Also, it has been reported that the ultraviolet irradiation is another effective manner to sharply shorten the desorption time of the adsorbed gas species.[61] Therefore, we assume that the Ni-PtS_2 monolayer is a promising reusable sensing material for gas detections.

It has been proved that the applied biaxial strains can modulate the constant lattice of the sensing material, therefore impacting its gas adsorption performance as well as the charge-transfer property, causing the variable sensing response accordingly.[62] Therefore, such an interesting phenomenon, in our opinion, should also be analyzed to explore the modulated sensing performance of the Ni-PtS_2 monolayer. In terms of the effect of the applied biaxial strains on the sensing behavior of the Ni-PtS_2 monolayer upon CO and C_2H_2 detection, Figure 6 describes the direction of applied biaxial strains as well as the varied Q_T and bandgap (B_g) with the variation of strains. At the same time, Figure 7 presents the MSC for CO and C_2H_2 adsorptions on the Ni-PtS_2 monolayer under some typical strains (−4, −2, +2, and +4%) to elucidate the geometric activation of two systems caused by the applied biaxial strains.

We define the compressive force as the negative strain and the drawing force as the positive strain, as presented in Figure 6a,b. From Figure 6c where dependences of Q_T and the applied biaxial strains for the two gas adsorption systems are shown, one could find that, with the increased strain in the positive direction, Q_T would be increased from the adsorbed gas species to the Ni-PtS_2 monolayer, while the increased biaxial strains in the negative direction can decrease the charge transfer in the same path. That is, the compressive force can enhance the charge transfer, whereas the drawing force can weaken the transfer transfer in the CO and C_2H_2 systems. In Figure 6d, we find that the relationship between the bandgap and the applied biaxial strains keeps a good linearity from −4 to +2% in the CO system and from −4 to +3% in the C_2H_2 system, wherein the bandgap gradually increases as the biaxial strain increases. However, when the applied biaxial strain exceeds the threshold value (2% for the CO system and 3% for the C_2H_2 system), the linear relation would disappear and the bandgaps of two gas systems sharply decrease, which may impact its sensing response for gas detection by modulating the biaxial strain from the positive direction. These finding regarding the adjustable Q_T and B_g prove the admirable potentials of the Ni-PtS_2 monolayer as a strain-tuned sensor for gas detections.[63] While for the CO and C_2H_2 sensing, the enhanced response could be obtained by the increase of the compressive force,

https://doi.org/10.1021/acsomega.3c00022
ACS Omega 2023, 8, 6090−6098

where the electrical resistance of the Ni-PtS_2 monolayer would decrease accordingly.

From Figure 7, it is found that the geometric structure of the Ni-PtS_2 monolayer is significantly deformed under the applied biaxial strains. Specifically, the S−S layer distance in two systems is widened to about 2.78 and 2.70 Å when the applied biaxial strains are −4 and −2% and is narrowed to about 2.55 and 2.48 Å when the applied biaxial strains are +4 and +2%. On the other hand, the MSC for CO and C_2H_2 adsorptions onto the Ni-PtS_2 surface is not largely impacted, wherein the Ni−C bonds are not distorted compared with those in the 0% strain counterparts (1.76 Å for the CO system and 1.93 Å for the C_2H_2 system). In other words, the applied biaxial strain can only exert somewhat geometric activations on the Ni-PtS_2 surface rather than the gas adsorption configurations. These findings confirm the desirable elastic property of the PtS_2 monolayer and its stable adsorption performance upon gas species.

3.6. Nonequilibrium Green's Function Analysis. To further discuss the current−voltage (I−V) properties of the Ni-PtS_2 monolayer, a theoretical sensing device was established containing a left electrode, a right electrode, and a scattering region. The length of the three regions is 6.13, 6.13, and 18.40 Å, respectively, and the vacuum layer is also 15 Å. The nonequilibrium Green's function with the PBE method is applied to investigate the transmission properties in Atomic Toolkit. The k point value is set as 1 × 3 × 100 at 300 K. The transmission current at different bias voltages is obtained based on the Landauer−Buttiker formula

$$I(V) = \frac{2e^2}{h}\int_{-\infty}^{\infty} T(E, V)[f(E - \mu_{\text{Left}}) - f(E - \mu_{\text{Right}})]\mathrm{d}E \quad (6)$$

where T is the transmission coefficient and h is the Planck constant. f denotes the Fermi−Dirac distribution function. μ_{Left} and μ_{Right} are the electrochemical potential of two electrodes.

The I−V curves of the Ni-PtS_2 monolayer before and after gas adsorptions are shown in Figure 8. When the voltage is smaller than 1.8 V, the current is low enough to be neglected. With the increase of bias voltage, the Ni-PtS_2 monolayer has the largest current, verifying its smallest resistance ranging at 3.1×10^5 to 5.7×10^7 Ω. While after the adsorption of CO or C_2H_2, its current decreases to different degrees with a sharper decrease in the CO system, suggesting its stronger sensitivity here, with voltage ranging at 2.0−2.4 V. These findings are in good accordance with the BS analysis and confirm that the Ni-PtS_2 monolayer has no selectivity upon CO and C_2H_2.

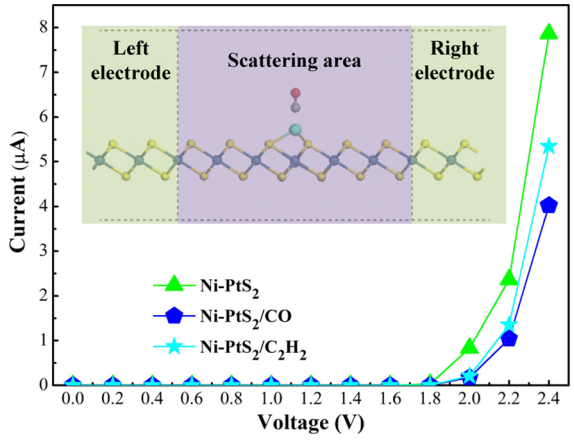

Figure 8. I−V curves of various systems with the device using the CO system for example.

4. CONCLUSIONS

In this work, the Ni-PtS_2 monolayer is proposed by the first-principles theory as a strain-modulated gas sensor for detections of CO or C_2H_2 in the oil-immersed transformer to value their operation conditions. The adsorption performance, related electronic behavior, and the effect of applied biaxial strain of the Ni-PtS_2 monolayer upon two gases are studied to investigate its potential to be a gas sensor. The main conclusions are seen as follows:

i. Ni decorating is quite stable on the PtS_2 monolayer with the E_b of −3.35 eV, which narrows the bandgap to 0.818 eV for the Ni-PtS_2 system, and the Ni dopant is strongly hybrid with the S and Pt atoms.
ii. Ni-PtS_2 monolayer performs chemisorption upon CO and C_2H_2, which leads to the significant change to its electronic property that gives its potential as a resistance-type sensor.
iii. The applied compressive force can activate the geometry of the Ni-PtS_2 monolayer and improve its sensing response upon two species, verifying its potential as a strain-modulated gas sensor.
iv. The I−V curves analysis confirms the BS analysis and the limited sensitivity upon two gas species.

In short, out theoretical calculations give a deep insight into the sensing property of the resistance-type Ni-PtS_2 monolayer gas sensor as a strain-modulated one. It is meaningful to further broaden the exploration and application of TMDs for gas sensing in many other fields.

AUTHOR INFORMATION

Corresponding Author

Zhuoli Xu − *Hubei Engineering Research Center for Safety Monitoring of New Energy and Power Grid Equipment, Hubei University of Technology, Wuhan 430068, China;*
orcid.org/0000-0002-4797-1299;
Email: xzl772010568@163.com

Complete contact information is available at:
https://pubs.acs.org/10.1021/acsomega.3c00022

Notes

The author declares no competing financial interest.

ACKNOWLEDGMENTS

This work was supported by the National Natural Science Foundation of China (no. 52207175).

REFERENCES

(1) Liao, R.; Zheng, H.; Grzybowski, S.; Yang, L.; Zhang, Y.; Liao, Y. An Integrated Decision-Making Model for Condition Assessment of Power Transformers Using Fuzzy Approach and Evidential Reasoning. *IEEE Trans. Power Delivery* **2011**, *26*, 1111−1118.
(2) Baek, D.-H.; Kim, J. MoS2 gas sensor functionalized by Pd for the detection of hydrogen. *Sens. Actuators, B* **2017**, *250*, 686.
(3) Ding, J.; Li, X.; Cao, J.; Sheng, L.; Yin, L.; Xu, X. New sensor for gases dissolved in transformer oil based on solid oxide fuel cell. *Sens. Actuators, B* **2014**, *202*, 232−239.
(4) Mak, T.; Westerwaal, R. J.; Slaman, M.; Schreuders, H.; van Vugt, A. W. V.; Victoria, M.; Boelsma, C.; Dam, B. Optical fiber sensor for the

continuous monitoring of hydrogen in oil. *Sens. Actuators, B* **2014**, *190*, 982−989.
(5) He, X.; Gui, Y.; Xie, J.; Liu, X.; Wang, Q.; Tang, C. A DFT study of dissolved gas (C2H2, H2, CH4) detection in oil on CuO-modified BNNT. *Appl. Surf. Sci.* **2020**, *500*, 144030.
(6) Yang, F.; Jung, D.; Penner, R. M. Trace Detection of Dissolved Hydrogen Gas in Oil Using a Palladium Nanowire Array. *Anal. Chem.* **2011**, *83*, 9472−9477.
(7) Ma, G. M.; Li, C. R.; Luo, Y. T.; Mu, R. D.; Wang, L. High sensitive and reliable fiber Bragg grating hydrogen sensor for fault detection of power transformer. *Sens. Actuators, B* **2012**, *169*, 195−198.
(8) Singh, S.; Bandyopadhyay, M. N. Dissolved gas analysis technique for incipient fault diagnosis in power transformers: A bibliographic survey. *IEEE Electr. Insul. Mag.* **2010**, *26*, 41−46.
(9) Zhang, G.; Zhang, X.; Cheng, H.; Tang, J. Ladder-wise calculation method for z-coordinate of transformer PD source based on planar layout UHF antenna sensors. *IEEJ Trans. Electr. Electron. Eng.* **2019**, *15*, 340.
(10) Benounis, M.; Aka-Ngnui, T.; Jaffrezic, N.; Dutasta, J. P. NIR and optical fiber sensor for gases detection produced by transformation oil degradation. *Sens. Actuators, A* **2008**, *141*, 76−83.
(11) Choi, S. Y.; Kim, Y.; Chung, H. S.; Kim, A. R.; Kwon, J. D.; Park, J.; Kim, Y. L.; Kwon, S. H.; Hahm, M. G.; Cho, B. Effect of Nb Doping on Chemical Sensing Performance of Two-Dimensional Layered MoSe2. *ACS Appl. Mater. Interfaces* **2017**, *9*, 3817−3823.
(12) Kazemi, A.; Rodner, M.; Fadavieslam, M. R.; Kaushik, P. D.; Ivanov, I. G.; Eriksson, J.; Syväjärvi, M.; Yakimova, R.; Yazdi, G. R. The effect of Cl- and N-doped MoS2 and WS2 coated on epitaxial graphene in gas-sensing applications. *Surf. Interfaces* **2021**, *25*, 101200.
(13) Li, F.; Asadi, H. DFT study of the effect of platinum on the H2 gas sensing performance of ZnO nanotube: explaining the experimental observations. *J. Mol. Liq.* **2020**, *309*, 113139.
(14) Zhang, Y.-H.; Yue, L.-J.; Gong, F.-L.; Li, F.; Zhang, H.-L.; Chen, J.-L. Highly enhanced H2S gas sensing and magnetic performances of metal doped hexagonal ZnO monolayer. *Vacuum* **2017**, *141*, 109−115.
(15) Zhang, X.; Lei, Y.; Xiaoqing, W.; Weihua, H. Experimental Sensing and Density Functional Theory Study of H2S and SOF2 Adsorption on Au-Modified Graphene. *Adv. Sci.* **2015**, *2*, 1500101.
(16) Zhang, X.; Yu, L.; Gui, Y.; Hu, W. First-principles study of SF6 decomposed gas adsorbed on Au-decorated graphene. *Appl. Surf. Sci.* **2016**, *367*, 259−269.
(17) Yar, M.; Hashmi, M. A.; Ayub, K. Nitrogenated holey graphene (C2N) surface as highly selective electrochemical sensor for ammonia. *J. Mol. Liq.* **2019**, *296*, 111929.
(18) Chen, G. X.; Li, H. F.; Wang, D. D.; Li, S. Q.; Fan, X. B.; Zhang, J. M. Adsorption of toxic gas molecules on pristine and transition metal doped hexagonal GaN monolayer: A first-principles study. *Vacuum* **2019**, *165*, 35−45.
(19) Chhowalla, M.; Shin, H. S.; Eda, G.; Li, L. J.; Loh, K. P.; Zhang, H. The chemistry of two-dimensional layered transition metal dichalcogenide nanosheets. *Nat. Chem.* **2013**, *5*, 263−275.
(20) Shokri, A.; Salami, N. Gas sensor based on MoS2 monolayer. *Sens. Actuators, B* **2016**, *236*, 378−385.
(21) Cao, W.; Zhao, Q.; Yang, L.; Cui, H. Enhanced NOx adsorption and sensing properties of MoTe2 monolayer by Ni-doping: A first-principles study. *Surf. Interfaces* **2021**, *26*, 101372.
(22) Cui, H.; Chen, D.; Zhang, Y.; Zhang, X. Dissolved gas analysis in transformer oil using Pd catalyst decorated MoSe2 monolayer: A first-principles theory. *Sustainable Mater. Technol.* **2019**, *20*, No. e00094.
(23) Cui, H.; Zhang, X.; Zhang, G.; Tang, J. Pd-doped MoS2 monolayer: A promising candidate for DGA in transformer oil based on DFT method. *Appl. Surf. Sci.* **2019**, *470*, 1035−1042.
(24) Manchanda, P.; Enders, A.; Sellmyer, D. J.; Skomski, R. Hydrogen-induced ferromagnetism in two-dimensional Pt dichalcogenides. *Phys. Rev. B* **2016**, *94*, 104426.
(25) Wu, D.; Jia, C.; Shi, F.; Zeng, L.; Lin, P.; Dong, L.; Shi, Z.; Tian, Y.; Li, X.; Jie, J. Mixed-dimensional PdSe2/SiNWA heterostructure based photovoltaic detectors for self-driven, broadband photodetection, infrared imaging and humidity sensing. *J. Mater. Chem. A* **2020**, *8*, 3632−3642.
(26) Zhang, D.; Yang, Z.; Li, P.; Pang, M.; Xue, Q. Flexible self-powered high-performance ammonia sensor based on Au-decorated MoSe2 nanoflowers driven by single layer MoS2-flake piezoelectric nanogenerator. *Nano Energy* **2019**, *65*, 103974.
(27) Tang, M.; Zhang, D.; Wang, D.; Deng, J.; Kong, D.; Zhang, H. Performance prediction of 2D vertically stacked MoS2-WS2 heterostructures base on first-principles theory and Pearson correlation coefficient. *Appl. Surf. Sci.* **2022**, *596*, 153498.
(28) Liu, G.; Yan, G.; Ruge, Q.; Pengfei, L. Strain dependent electronic and optical properties of PtS2 monolayer. *Chem. Phys. Lett.* **2018**, *709*, 65−70.
(29) Huang, Z.; Wenxu, Z.; Wanli, Z. Computational Search for Two-Dimensional MX2 Semiconductors with Possible High Electron Mobility at Room Temperature. *Materials* **2016**, *9*, 716.
(30) Fan, Y.; Zhang, J.; Qiu, Y.; Zhu, J.; Zhang, Y.; Hu, G. A DFT study of transition metal (Fe, Co, Ni, Cu, Ag, Au, Rh, Pd, Pt and Ir)-embedded monolayer MoS2 for gas adsorption. *Comput. Mater. Sci.* **2017**, *138*, 255−266.
(31) Wu, P.; Yin, N.; Li, P.; Cheng, W.; Huang, M. The adsorption and diffusion behavior of noble metal adatoms (Pd, Pt, Cu, Ag and Au) on a MoS2 monolayer: a first-principles study. *Phys. Chem. Chem. Phys.* **2017**, *19*, 20713.
(32) Liu, X.; Liu, J.; Yang, H.; Huang, B.; Zeng, G. Design of a high-performance graphene/SiO2-Ag periodic grating/MoS2 surface plasmon resonance sensor. *Appl. Opt.* **2022**, *61*, 6752−6760.
(33) Zhu, H.; Zhao, R. Isolated Ni atoms induced edge stabilities and equilibrium shapes of CVD-prepared hexagonal boron nitride on the Ni (111) surface. *New J. Chem.* **2022**, *46*, 17496−17504.
(34) Zhang, K.-Q.; Deng, Q.-F.; Luo, J.; Gong, C.-L.; Chen, Z.-G.; Zhong, W.; Hu, S.-Q.; Wang, H.-F. Multifunctional Ag (I)/CAAA-Amidphos Complex-Catalyzed Asymmetric [3+ 2] Cycloaddition of α-Substituted Acrylamides. *ACS Catal.* **2021**, *11*, 5100−5107.
(35) Pan, Q.; Li, T.; Zhang, D. Ammonia gas sensing properties and density functional theory investigation of coral-like Au-SnSe2 Schottky junction. *Sens. Actuators, B* **2021**, *332*, 129440.
(36) Huo, J.; Wei, H.; Fu, L.; Zhao, C.; He, C. Highly active Fe36Co44 bimetallic nanoclusters catalysts for hydrolysis of ammonia borane: The first-principles study. *Chin. Chem. Lett.* **2023**, *34*, 107261.
(37) Cui, H.; Zhang, X.; Li, Y.; Chen, D.; Zhang, Y. First-principles insight into Ni-doped InN monolayer as a noxious gases scavenger. *Appl. Surf. Sci.* **2019**, *494*, 859−866.
(38) Zhou, X.; Chu, W.; Zhou, Y.; Sun, W.; Xue, Y. DFT simulation on H2 adsorption over Ni-decorated defective h-BN nanosheets. *Appl. Surf. Sci.* **2018**, *439*, 246−253.
(39) Cui, H.; Yan, C.; Jia, P.; Cao, W. Adsorption and sensing behaviors of SF6 decomposed species on Ni-doped C3N monolayer: A first-principles study. *Appl. Surf. Sci.* **2020**, *512*, 145759.
(40) Zhang, D.; Wu, J.; Li, P.; Cao, Y. Room-temperature SO2 gas-sensing properties based on a metal-doped MoS2 nanoflower: an experimental and density functional theory investigation. *J. Mater. Chem. A* **2017**, *5*, 20666−20677.
(41) Li, P.; Hong, Q.; Wu, T.; Cui, H. SOF2 sensing by Rh-doped PtS2 monolayer for early diagnosis of partial discharge in the SF6 insulation device. *Mol. Phys.* **2021**, *119*, No. e1919774.
(42) Grimme, S. Semiempirical GGA-type density functional constructed with a long-range dispersion correction. *J. Comput. Chem.* **2006**, *27*, 1787−1799.
(43) Tkatchenko, A.; DiStasio, R. A., Jr.; Head-Gordon, M.; Scheffler, M. Dispersion-corrected Møller-Plesset second-order perturbation theory. *J. Chem. Phys.* **2009**, *131*, 094106.
(44) Yang, S.; Lei, G.; Xu, H.; Xu, B.; Li, H.; Lan, Z.; Wang, Z.; Gu, H. A DFT study of CO adsorption on the pristine, defective, In-doped and Sb-doped graphene and the effect of applied electric field. *Appl. Surf. Sci.* **2019**, *480*, 205−211.
(45) Monkhorst, H. J.; Pack, J. D. Special points for Brillouin-zone integrations. *Phys. Rev. B: Solid State* **1976**, *13*, 5188−5192.

https://doi.org/10.1021/acsomega.3c00022
ACS Omega 2023, 8, 6090−6098

(46) Wu, H.; Xia, Y.; Zhang, C.; Xie, S.; Wu, S.; Cui, H. Adsorptions of C5F10O decomposed compounds on the Cu-decorated NiS2 monolayer: a first-principles theory. *Mol. Phys.* **2023**, No. 25, No. e2163715.
(47) Ju, W.; Li, T.; Su, X.; Li, H.; Li, X.; Ma, D. Au cluster adsorption on perfect and defective MoS2 monolayers: structural and electronic properties. *Phys. Chem. Chem. Phys.* **2017**, *19*, 20735.
(48) Shokuhi Rad, A.; Zareyee, D. Adsorption properties of SO2 and O3 molecules on Pt-decorated graphene: A theoretical study. *Vacuum* **2016**, *130*, 113−118.
(49) Ji, Y.; Liu, Y.; Xu, Y.; Liu, L.; Chen, Y. Electronic and optical properties of sulfur vacancy-defect monolayer PtS2: A first-principles study. *Mater. Chem. Phys.* **2020**, *255*, 123588.
(50) Cui, H.; Jia, P.; Peng, X. Adsorption of SO2 and NO2 molecule on intrinsic and Pd-doped HfSe2 monolayer: A first-principles study. *Appl. Surf. Sci.* **2020**, *513*, 145863.
(51) Miró, P.; Ghorbani-Asl, M.; Heine, T. Two Dimensional Materials Beyond MoS2 : Noble-Transition-Metal Dichalcogenides. *Angew. Chem., Int. Ed.* **2014**, *53*, 3015−3018.
(52) Cui, H.; Liu, T.; Zhang, Y.; Zhang, X. Ru-InN Monolayer as a Gas Scavenger to Guard the Operation Status of SF6 Insulation Devices: A First-Principles Theory. *IEEE Sens. J.* **2019**, *19*, 5249−5255.
(53) Huang, J.; Chu, J.; Wang, Z.; Zhang, J.; Yang, A.; Li, X.; Gao, C.; Huang, H.; Wang, X.; Cheng, Y.; Rong, M. Chemisorption of NO2 to MoS2 Nanostructures and its Effects for MoS2 Sensors. *ChemNanoMat* **2019**, *5*, 1123−1130.
(54) Gui, Y.; Li, W.; He, X.; Ding, Z.; Tang, C.; Xu, L. Adsorption properties of pristine and Co-doped TiO2(1 0 1) toward dissolved gas analysis in transformer oil. *Appl. Surf. Sci.* **2020**, *507*, 145163.
(55) Cui, H.; Zhang, X.; Zhang, J.; Zhang, Y. Nanomaterials-based gas sensors of SF6 decomposed species for evaluating the operation status of high-voltage insulation devices. *High Voltage* **2019**, *4*, 242−258.
(56) Zhou, Q.; Zhang, G.; Tian, S.; Zhang, X. First-Principles Insight into Pd-Doped ZnO Monolayers as a Promising Scavenger for Dissolved Gas Analysis in Transformer Oil. *ACS Omega* **2020**, *5*, 17801−17807.
(57) Gui, Y.; Shi, J.; Li, T.; Tang, C.; Xu, L. Platinum modified MoS2 monolayer for adsorption and gas sensing of SF6 decomposition products: A DFT study. *High Voltage* **2019**, *5*, 454.
(58) Donarelli, M.; Prezioso, S.; Perrozzi, F.; Bisti, F.; Nardone, M.; Giancaterini, L.; Cantalini, C.; Ottaviano, L. Response to NO2 and other gases of resistive chemically exfoliated MoS2-based gas sensors. *Sens. Actuators, B* **2015**, *207*, 602−613.
(59) Zhang, Y.-H.; Chen, Y.-B.; Zhou, K.-G.; Liu, C.-H.; Zeng, J.; Zhang, H.-L.; Peng, Y. Improving gas sensing properties of graphene by introducing dopants and defects: a first-principles study. *Nanotechnology* **2009**, *20*, 185504.
(60) Peng, S.; Cho, K.; Qi, P.; Dai, H. Ab initio study of CNT NO2 gas sensor. *Chem. Phys. Lett.* **2004**, *387*, 271−276.
(61) Feng, Z.; Xie, Y.; Chen, J.; Yu, Y.; Zheng, S.; Zhang, R.; Li, Q.; Chen, X.; Sun, C.; Zhang, H.; Pang, W.; Liu, J.; Zhang, D. Highly sensitive MoTe2 chemical sensor with fast recovery rate through gate biasing. *2D Mater.* **2017**, *4*, 025018.
(62) Wang, D.; Lan, T.; Pan, J.; Liu, Z.; Yang, A.; Yang, M.; Chu, J.; Yuan, H.; Wang, X.; Li, Y. J.; Rong, M. Janus MoSSe monolayer: A highly strain-sensitive gas sensing material to detect SF6 decompositions. *Sens. Actuators, A* **2020**, *311*, 112049.
(63) Jin, C.; Tang, X.; Tan, X.; Smith, S. C.; Dai, Y.; Kou, L. A Janus MoSSe monolayer: a superior and strain-sensitive gas sensing material. *J. Mater. Chem. A* **2019**, *7*, 1099−1106.

https://doi.org/10.1021/acsomega.3c00022
ACS Omega 2023, 8, 6090−6098